

# Spectroscopic survey of $\delta$ Scuti stars

## I. Rotation velocities and effective temperatures<sup>\*</sup>

E. Solano<sup>1</sup> and J. Fernley<sup>2</sup>

<sup>1</sup> INSA, ESA-IUE Observatory, P.O. Box 50727, 28080 Madrid, Spain

<sup>2</sup> IUE Observatory, P.O. Box 50727, 28080 Madrid, Spain

Received January 2; accepted July 19, 1996

**Abstract.** Projected rotational velocities and effective temperatures for 68  $\delta$  Sct stars as well as 41 non-variable stars of similar spectral type and luminosity are presented here. The rotational velocities have been calculated following the method developed in Gray (1992) and effective temperatures have been derived using the Balmer line profiles. The temperatures obtained from this method are shown to be in reasonable agreement with those calculated using the Infrared Flux Method (IRFM) or spectrophotometric methods. This result has allowed us to use our temperatures to compare different  $uvby\beta$  photometric calibrations. We find that the calibration given by Moon & Dworetzky (1985) is the most consistent. In the second part of this paper we have studied the relation between the pulsational properties (periods and amplitudes) and the physical parameters ( $v \sin i$  and  $T_{\text{eff}}$ ). Where pulsation modes have been determined, the low amplitude  $\delta$  Scutis tend to be multimode (radial and non-radial) pulsators, consistent with the theory that non-linear coupling between modes acts to limit the amplitude in these stars. We have compared the distribution of  $v \sin i$  for low amplitude  $\delta$  Scutis and non-variable stars. This shows the  $\delta$  Scutis have a broader distribution in  $v \sin i$  suggesting that a high rotation velocity may favour pulsation. We find that the large amplitude  $\delta$  Scuti stars tend to have longer periods, cooler temperatures and lower rotation velocities. Given that the large amplitude stars are also relatively rare all the above are consistent with the hypothesis that these stars are more evolved (sub-giants) than the low amplitude  $\delta$  Scutis (main sequence or early post-main sequence).

**Key words:** stars: rotation — stars: fundamental parameters — stars: variables:  $\delta$  Sct

### 1. Introduction

$\delta$  Sct stars form the second most numerous group of pulsators in the Galaxy after the pulsating white dwarfs. They are located in the lower part of the instability strip and have spectral types A–F and a range of luminosities that extends from the Main Sequence to two magnitudes above it. These stars are characterized by having periods shorter than 0<sup>d</sup>.3, amplitudes ranging from some thousandths of magnitude to some tenths and complicated light curves that can vary with time (Rodríguez et al. 1994). Some  $\delta$  Sct stars are known to be in binary systems. The pulsation behaviour ranges from single-mode radial or multimode radial to mixed radial/non-radial oscillations. Pulsation does not seem to be related to age since  $\delta$  Scuti stars are found in clusters as young as 10<sup>6</sup> yr. and in older disk population groups such as  $\sigma$  Pup (Eggen 1971).

Although in the past those stars with large amplitudes were called *dwarf Cepheids* (Smith 1955), *AI Vel* (Bessel 1969) and *RRs stars* (Kukarkin et al. 1969), nowadays it is widely accepted that in their physical characteristics they resemble the low amplitude  $\delta$  Sct stars (e.g. McNamara & Feltz 1978; Breger 1980). Whilst most  $\delta$  Scutis belong to Population I there is a small group that belong to Population II. They are called *SX Phe* stars or variable blue stragglers (Eggen & Iben 1989; Nemeč & Mateo 1990). In this work, those Population I stars with amplitudes greater than 0<sup>m</sup>.1 will be simply referred to as *large amplitude  $\delta$  Scuti stars*.

In the last years most work on  $\delta$  Sct stars has been devoted to the identification of pulsational modes from photometric observations (see, for instance, the series of papers by Poretti et al. (1992 and references therein) and

Send offprint requests to: E. Solano; esm@vilspa.esa.es

\* Tables 3 and 4 are also available in electronic form. Tables 6 and 7 are only available in electronic form via ftp 130.79.128.5 or <http://cdsweb.u-strasbg.fr/Abstract.html>

**Table 1.** Program  $\delta$  Scuti stars. The identification, magnitude, spectral type and pulsational parameters are from Rodríguez et al. (1994) except for those cases where the star is marked with \* where García et al. (1993) was used. The last column indicates the telescope where the observations were done (2.1 means 2.1 meters telescope at McDonald). The number in parenthesis indicates the number of spectra observed with each telescope. The pulsation mode is given by  $F$  (fundamental radial mode),  $nH$  ( $n^{\text{th}}$  overtone),  $R$  (radial pulsation),  $NR$  (non-radial pulsation),  $nr$  (non-radial pulsation not clearly stated)

HD	Identificación		$V$	Period (days)	Amplitude ( $\Delta V$ )	Mode	Spectral type	Telescope
	HR	GCVS						
432	21	$\beta$ Cas	2.27	0.1009	0.033	$NR^{(1)}$	F2 II-IV	JKT
		V377 Cas	7.83	0.0300	0.050		F0	JKT
2628	114	GN And	5.23	0.0693	0.050	$NR^{(2)}$	A7 III	JKT-2.1
4818	238	V526 Cas	6.39	0.0396	0.010		F2 IV	JKT-2.1
8511	401	AV Cet	6.21	0.0685	0.010	$F - 1H^{(3)}$	F0 V	JKT
9100	432	VX Psc	6.02	0.1360	0.020		A4 IV	JKT (2)
10845	515	VY Psc	6.55	0.2190	0.020		A9 III	JKT
11285		VV Ari	6.69	0.0764	0.020		F0	JKT
15165		VW Ari	6.71	0.1071	0.060	$F - 1H - 2H - NR^{(4)}$	F0 IV	JKT
15550	729	UU Ari	6.15	0.0676	0.010	$NR^{(5)}$	A9 V	JKT
17093	812	UV Ari	5.22	0.0355	0.040		A7 IV	JKT
23156		V624 Tau	8.23	0.0210	0.010		A7 V	JKT
23567		V534 Tau	8.40	0.0320	0.015		A9 V	JKT
23728	1170	V376 Per	6.02	0.0994	0.070	$R - nr^{(6)}$	A9 IV	JKT (2)
24550		V479 Tau	7.44	0.0758	0.030		F3 II-III	JKT
24809	1223	V386 Per	6.53	0.0550	0.010		A8 V	JKT
24832	1225	DI Eri	6.19	0.1559	0.050	$R - NR^{(7)}$	F1 V	JKT
26322	1287	IM Tau	5.41	0.1450	0.070	$F, 1H, 2H, NR^{(8)}$	F2 IV	JKT-2.1 (2)
26574	1298	$o$ Eri	4.04	0.0747	0.030	$R - NR^{(7)}$	F2 II-III	JKT
27397	1351	V483 Tau	5.59	0.0540	0.020		F0 IV	JKT
27459	1356	V696 Tau	5.26	0.0360	0.010		A9 IV	JKT
27628	1368	V775 Tau	5.72	0.0630	0.010		F2III <sub>m</sub>	JKT-2.1
28024	1392	$v$ Tau	4.28	0.1484	0.016	$R^{(9)}$	A8 V	JKT
28052	1394	V777 Tau	4.48	0.1630	0.020		A8 V	JKT (2)
28319	1412	TH2 Tau	3.42	0.0756	0.020	$NR^{(10)}$	A7 III	JKT
28910	1444	$\rho$ Tau	4.66	0.0670	0.010		A8 V	JKT
30780	1547	V480 Tau	5.10	0.0420	0.012		A7 IV-V	JKT
33959	1706	KW Aur	5.02	0.0881	0.080	$R - NR^{(11)}$	A9 IV	JKT-2.1 (2)
37819		V356 Aur	8.06	0.1893	0.080	$R - nr^{(12)}$	F8 III <sub>p</sub>	JKT (2)-2.1
40372	2100	V1004 Ori	5.90	0.0540	0.010		A5 <sub>m</sub>	JKT
40535	2107	V474 Mon	6.12	0.1361	0.150	$R - NR^{(13)}$	F2 V	JKT(2)-2.1 (2)
		UZ Lyn (*)	4.58				A2 V	JKT (2)
50018	2539	OX Aur	6.12	0.1547	0.030	$F - 1H^{(14)}$	F2 V	JKT (2)
50420	2557	V352 Aur	6.13	0.1700	0.010	$R - nr^{(15)}$	A9 III	JKT-2.1
55057	2707	V571 Mon	5.45	0.1000	0.050	$NR^{(16)}$	F0 V	JKT
64191		AD CMi	0.38	0.1230	0.300	$F^{(17)}$	F3 III	INT (2)-2.1 (2)
73857		VZ Cnc	7.65	0.1784	0.500	$1H^{(18)}$	F2 III	JKT (2)-2.1 (2)
110377	4824	GG Vir	6.19	0.0500	0.020	$F, 1H, 2H, 3H^{(19)}$	A8 V	INT
152830	6290	V644 Her	6.34	0.1151	0.040		F3 V	JKT-2.1
152896		V645 Her	7.37				A5	JKT (2)
155514	6391	V620 Her	6.19	0.0884	0.020	$F, NR^{(20)}$	A8 V	JKT
156697	6434	V2112 Oph	6.51	0.1874	0.020	$F, 1H^{(21)}$	F1 V	JKT
159223		V648 Her	6.88	0.2900			A7 V	JKT
172748	7020	$\delta$ Scut	4.72	0.1938	0.290	$R, NR^{(22)}$	F2 III	JKT (2)
177392	7222	LT Vul	6.52	0.1096	0.030	$2H - 3H^{(23)}$	F2 III	JKT
181333	7331	V1208 Aql	5.50	0.1497	0.040	$F - nr^{(23)}$	F0 III	JKT
181577	7340	$\rho$ I Sgr	3.94	0.0500	0.020		F0 III-IV	JKT
186357	7501	V1276 Cyg	6.52	0.0880	0.020		F1 III	JKT
192518	7731	NU Vul	5.20	0.1881	0.016		A7 IV	JKT
197461	7928	$\delta$ Del	4.43	0.1568	0.070	$R - nr^{(24)}$	F0 IV	JKT (2)
199124	8006	EM Aqr	6.55	0.0990	0.020		A9 V	JKT
199908		DQ Cep	7.22	0.0789	0.050	$F, 2H^{(25)}$	F1 IV	JKT
200356		FN Aqr (*)	7.30		0.010			JKT
200925		V1719 Cyg	8.01	0.2673	0.310	$R^{(26)}$	F2 III	JKT (2)
201707	8102	EW Aqr	6.49	0.0970	0.070	$NR^{(27)}$	F0 III	JKT
204188	8210	IK Peg	6.07	0.0440	0.010	$F - NR^{(28)}$	A8 <sub>m</sub>	JKT
211336	8494	$\epsilon$ Cep	4.19	0.0412	0.014	$NR^{(29)}$	F0 IV	JKT
213534	8584	GX Peg	6.35	0.0560	0.015	$R - NR^{(30)}$	A5 <sub>m</sub>	JKT
215874	8676	FM Aqr	6.19	0.0870	0.020		A9 III-IV	JKT

Table 1. continued

HD	Identificación		V	Period (days)	Amplitude ( $\Delta V$ )	Mode	Spectral type	Telescope
	HR	GCVS						
218549		DY Peg	10.36	0.0729	0.540	$F^{(31)}$	A9	INT (2)-2.1 (2)
		CC And	9.39	0.1249	0.240	$F, 1H, 2H, NR^{(32)}$	F3 IV-V	INT (2)-2.1 (2)
		GP And	10.80	0.0787	0.520	$R^{(33)}$	A3	INT-2.1 (2)
		AI Hya	9.90	0.1380	0.020		F5	INT
		CY Aqr	10.93	0.0610	0.710	$R^{(34)}$	A2-F8	INT (2)
		DE Lac	10.28	0.2537	0.350		F5-F8	INT
		V1162 Ori	9.88	0.0787	0.180	$R^{(35)}$	A6	INT-2.1 (3)
		EH Lib	9.85	0.0880	0.500	$R^{(18)}$	F0	INT-2.1 (2)
		YZ Boo	10.57	0.1040	0.420	$F^{(18)}$	A6-F1	INT (2)-2.1(2)

1: Rodríguez et al. (1992a); 2: Rodríguez et al. (1993b); 3: González-Bedolla et al. (1990); 4: McNamara et al. (1984); 5: Ostermann et al. (1991); 6: Ostermann (1990); 7: Poretti (1989); 8: Poretti et al. (1992); 9: Bossi et al. (1983); 10: Breger et al. (1989); 11: Smith (1992); 12: Poretti et al. (1987); 13: Balona & Stobie (1980); 14: Gupta (1980); 15: Bossi et al. (1983); 16: Walker et al. (1987); 17: Yang (1992); 18: Fernley et al. (1987); 19: Bartolini et al. (1980); 20: Breger et al. (1994); 21: Breger (1982); 22: Coates et al. (1982); 23: Reed et al. (1988); 24: Uyaniker & Haykal (1991); 25: Pena et al. (1983); 26: Poretti et al. (1988); 27: Hobart et al. (1989); 28: Wonnacott et al. (1994); 29: Baade et al. (1992); 30: Michel et al. (1992); 31: Nemeč et al. (1994); 32: Fu et al. (1995); 33: Rodríguez et al. (1993a); 34: Powell et al. (1995); 35: Poretti et al. (1990).

Rodríguez et al. 1993a, b). Relatively little spectroscopic analysis has been done, even though the  $\delta$  Sct stars, especially the low amplitude ones, are bright objects.

The goal of this paper is to derive, using spectroscopic techniques, accurate values of the effective temperature and rotational velocities of the sample of  $\delta$  Sct and non-variable stars given in Tables 1 and 2 and to relate them with the pulsational parameters, period and amplitude. In particular we are interested in looking at differences between large and small amplitude pulsators. The cut-off amplitude below which a star may be considered small amplitude and above which it may be considered large amplitude is somewhat arbitrary. Breger (1979) presented a frequency–amplitude histogram and based on this we adopt a value of  $0^m1$  for the cut-off. In a second paper a detailed abundance analysis of iron, calcium and oxygen will be presented for the same sample of stars.

## 2. Observations and data reduction

The observations were performed in different observing runs carried out from 1990 to 1994 at two different observatories: the Observatorio del Roque de los Muchachos (La Palma, Spain) and the McDonald Observatory (Texas, U.S.A.).

Two telescopes were used in the Observatorio del Roque de los Muchachos: the 1.0 m Jakobus Kapteyn Telescope (hereafter referred to as JKT) and the 2.5 m Isaac Newton Telescope (hereafter, INT). In the first case we used the Richardson–Brealey spectrograph working with a  $385 \times 578$  pixels GEC CCD detector whereas the Intermediate Dispersion Spectrograph together with an  $1280 \times 1180$  pixels EEV5 CCD detector was used for the observations done with the INT. In both cases, the wavelength range covers  $\approx 200 \text{ \AA}$  ( $4790 \text{ \AA} - 5000 \text{ \AA}$ ) nearly centered at  $H\beta$ . The resolving power was 12 000 for the JKT and 13 000 for the INT which correspond to a recip-

rocal spectral dispersion of 0.41 and 0.37  $\text{\AA}/\text{pixel}$  at  $H\beta$  respectively.

Those stars with  $v \sin i \leq 40 \text{ km s}^{-1}$  observed in La Palma were further observed at the McDonald Observatory with the 2.1 m telescope using the Sandiford echelle spectrograph together with a  $1200 \times 400$  Reticon CCD. The covered spectral range was  $6190 \text{ \AA} - 8500 \text{ \AA}$  and the resolving power 110 000 which corresponds to a reciprocal spectral dispersion of 0.06  $\text{\AA}/\text{pixel}$  at  $H\alpha$ .

La Palma spectra were reduced using the MIDAS 1-D image reduction package: Firstly, the cosmic rays were removed by replacing the number of counts in the affected pixel(s) by the mean of the neighboring pixels. The raw spectra were then bias-subtracted, flatfield-corrected, (two or more master flatfield exposures were taken at the beginning of every night) and background-subtracted. The 1-D spectra were then extracted using the optimal extraction algorithm as proposed by Horne (1986). Since we were not interested in deriving radial velocities the wavelength calibration was made using the stellar spectral lines themselves and fitting a first-order polynomial. Wavelengths were taken from Moore et al. (1966). The continuum windows were chosen with the aid of the *Atlas of Procyon* (Griffin & Griffin 1979) and the continuum level calculated by fitting a third-degree polynomial. The normalized spectra were derived by dividing the extracted spectra by this continuum level. A typical S/N ratio of 150–200 was reached both in the JKT and in the INT observations whereas S/N ratios ranging from 50 to 190 were achieved in the McDonald observations. The S/N ratio was determined by measuring the standard deviation of the intensity of the normalized spectrum in a spectral window free of absorption lines.

The reduction of the McDonald spectra was performed under the context *echelle* within the MIDAS reduction package. A typical session of echelle reduction comprises the following steps: removal of wrong columns and saturated pixels, bias subtraction, spatial positioning of the

**Table 2.** Program non-variable stars. The identification,  $V$  magnitude and spectral type were obtained from *Centre de Données Stellaires* (CDS) using SIMBAD. The last column indicates the telescope where the observation was made (2.1 means 2.1 meters telescope at McDonald Observatory)

Identification HD	HR	$V$	Spectral type	Telescope	Identification HD	HR	$V$	Spectral type	Telescope
905	41	5.72	F0 IV	JKT	203803	8190	5.70	F1 IV	JKT
1671	82	5.18	F5 III	JKT-2.1	203842	8191	6.30	F5 III	JKT
4568	217	6.60	F8 V	JKT-2.1	203925	8198	5.70	A8 III	JKT
4757	230	7.00	F4 III	JKT	204153	8208	5.60	F0 V	JKT
4758	231	7.10	F5 III	JKT	205852	8267	5.40	F1 IV	JKT
6397	308	5.68	F4 II-III	JKT-2.1	205924	8270	5.70	A9 IV-V	JKT
7034	349	5.16	F0 V	JKT	207652	8344	5.29	F2 III-IV	JKT
8723	413	5.38	F2 V	JKT-2.1	210459	8454	4.29	F5 III	JKT
11257	534	5.90	F2 V	JKT-2.1	210594	8460	6.30	A8 IV	JKT
11636	553	2.64	A5 V	JKT	210855	8472	5.20	F8 V	JKT
11973	569	4.79	F0 V	JKT	214454	8613	4.63	A8 IV	JKT
13041	620	4.80	A5 IV-V	JKT	216048	8681	6.54	F0 IV-V	JKT
13161	622	3.00	A5 III	JKT	217754	8765	6.57	F2 IV	JKT-2.1
13174	623	4.98	F2 III	JKT	217926	8776	6.41	F2 V	JKT
15385	723	6.19	A5m	JKT-2.1	218396	8799	5.99	A5 V	JKT-2.1
16647	783	6.25	F3 V	JKT-2.1	218470	8805	5.70	F5 V	JKT-2.1
23230	1135	3.80	F5 IV	JKT-2.1	219080	8830	4.52	F0 V	JKT
24357	1201	6.00	F4 V	JKT	219291	8838	6.41	F6 IV	JKT
201507	8095	6.45	F5 IV	JKT	219487	8845	6.60	F5 V	JKT-2.1
202240	8120	6.00	F0 III	JKT	220242	8888	6.60	F5 V	JKT-2.1
202444	8130	3.72	F0 IV	JKT					

different spectral orders, flatfield correction, order extraction and wavelength calibration. The sky contribution was found not to be significant and no background subtraction was done. Although the ripple effect is an interference pattern inside the detector that depends on the angle of the rays entering the detector it was seen that the flatfield correction was enough to remove an important part of this effect permitting a linear fit to the spectral continuum. The wavelength calibration and continuum normalization were similar to those of La Palma spectra.

### 3. Determination of rotational velocities

There are several factors to be considered when a spectral line is selected for measuring rotation velocities.

- The main source of broadening must be rotation thus Balmer lines and strong lines for which the pressure broadening is comparable with the rotational broadening must be excluded.
- Weak lines that could disappear with increasing rotational velocity must also not be used.
- The lines must lie in a spectral region which permits an accurate determination of the continuum level in order to avoid systematic errors in the measurements of the line width.
- The lines must be unblended.

Very few lines fulfil these conditions in the La Palma spectra, mainly because of their moderate resolution which makes most of the lines appear blended. After a careful selection, we have chosen two lines: Fe I  $\lambda 4957.613 \text{ \AA}$  and Fe I  $\lambda 4988.955 \text{ \AA}$ . The first one

is stronger but it appears slightly blended with the weak line Fe I  $\lambda 4957.307 \text{ \AA}$  and it will be used only for  $v \sin i \geq 40 \text{ km s}^{-1}$  where it is not possible to use the weaker line Fe I  $\lambda 4988.955 \text{ \AA}$ . On the contrary, this problem is not present in the McDonald spectra where the spectral resolution is a factor of six higher. For these spectra, a set of nine lines was used in the calculation of the rotational velocities: Fe I  $\lambda 6265.141 \text{ \AA}$ , Fe I  $\lambda 6336.830 \text{ \AA}$ , Fe I  $\lambda 6393.612 \text{ \AA}$ , Fe I  $\lambda 6411.658 \text{ \AA}$ , Ca I  $\lambda 6439.083 \text{ \AA}$ , Ca I  $\lambda 6449.820 \text{ \AA}$ , Fe I  $\lambda 6677.997 \text{ \AA}$ , Ca I  $\lambda 6717.687 \text{ \AA}$  and Ca I  $\lambda 7148.150 \text{ \AA}$ .

Different techniques have been developed to calculate rotational velocities (e.g. Sletteback 1975; Tonry & Davis 1979; Gray 1992). Each one of these three methods relies to some extent on the geometrical technique, suggested originally by Shajn & Struve (1929), that relates line profiles and line widths to apparent rotational velocity,  $v \sin i$ . Collins & Truax (1995) noted that this technique implies the following three assumptions:

- The observational aspect of a uniformly rotating star may be approximated by a circular disk subject to a linear limb-darkening law applicable to all parts of the stellar disk.
- The limb-darkening law for the line is the same as for the continuum.
- The form of the line does not change over the apparent disk.

Under these assumptions, the standard rotation profile has the following form (Gray 1992)

$$G(\Delta\lambda) = (2(1 - \epsilon)[1 - (\Delta\lambda/\Delta\lambda_1)^2]^{1/2} + 1/2\pi\epsilon[1 - (\Delta\lambda/\Delta\lambda_1)^2]/(\pi\Delta\lambda_1(1 - \epsilon/3)) \quad (1)$$

where  $\Delta\lambda_1 = \lambda \cdot v \cdot \sin i / c$  represents the maximum broadening and  $\epsilon$  is the limb darkening coefficient. In this paper we will follow the method described by Gray (1992) since contrary to the Sletteback and Tonry & Davis methods which need to build up a calibration of rotational velocities according to some parameter (e.g. the FWHM in Sletteback), the Gray method provides direct and independent measurements of  $v \sin i$ . With this method the projected rotational velocity ( $v \sin i$ ) is calculated from the Eq. (17.14) given in Gray (1992) which relates the frequencies where the Fourier transform of  $G(\Delta\lambda)$  reaches a relative minimum and the wavelength of the line considered. This method is independent of the instrumental profile since the convolution of the intrinsic spectrum with the instrumental profile may add relative minimum values but will not change the position of the minima given by Eq. (17.14). Moreover, these minima introduced by the instrumental profile appear at much higher frequencies than those of the intrinsic spectrum used to calculate the rotational velocity. Projected rotational velocities of the observed stars are listed in Tables 3 and 4.

### 3.1. Estimated uncertainties in the calculated values of $v \sin i$

According to Eq. (1), one of the uncertainties in the calculation of  $v \sin i$  comes from the limb-darkening law. In our calculations, we have assumed a linear limb-darkening law in the form

$$I(\mu) = I(1)(1 - \epsilon(1 - \mu)) \quad (2)$$

where  $\mu = \cos \theta$  with  $\theta$  the angle formed by the line of sight and the direction of the emerging flux,  $I(1)$  represents the intensity at the stellar disk center and  $\epsilon$ , the linear limb-darkening coefficient, takes a value of  $\epsilon = 0.6$ . Although some authors (Klinglesmith & Sobieski 1970; Manduca et al. 1977; Díaz-Cordovés & Giménez 1992) have proposed different non-linear laws for limb darkening, Díaz-Cordovés & Giménez (1992) also showed that the errors in the total emergent flux assuming a linear law are less than 2% in the range of temperatures where the  $\delta$  Sct stars lie (6 000 K – 8 500 K).

Wade & Rucinski (1985) have tabulated the linear limb-darkening coefficient in terms of wavelength,  $T_{\text{eff}}$  and  $\log g$ . Assuming an interval of temperatures 6 500 K – 8 500 K,  $\log g = 4.0$  and spectral ranges of  $\lambda\lambda 4790 - 5 000 \text{ \AA}$  (La Palma) and  $\lambda\lambda 6190 - 8 500 \text{ \AA}$  (McDonald) we obtain  $0.53 \leq \epsilon \leq 0.63$  for La Palma spectra and  $0.33 \leq \epsilon \leq 0.53$  for McDonald spectra.

To see to what extent the limb-darkening coefficient affects the calculated value of  $v \sin i$ , we have convolved a synthetic line (Fe I  $\lambda = 6252 \text{ \AA}$ ), generated with ATLAS8 and with null rotational broadening by definition, with a grid of rotational profiles ( $v \sin i = 30, 60, 90, 120, 150, 180 \text{ km s}^{-1}$ ) and we have calculated the rotational velocity for two values of  $\epsilon$  (0.3, 0.6) which would correspond to the

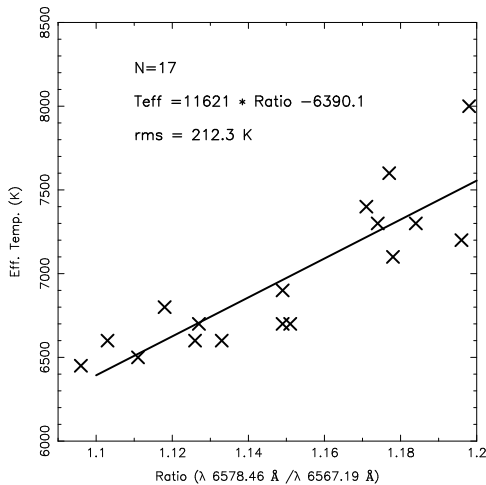
**Table 3.** Rotational velocities of observed  $\delta$  Sct stars. The fourth column indicates the value of  $v \sin i$  obtained using the method described in Gray (1992). For La Palma spectra, the line chosen for the  $v \sin i$  calculation appears in the last column. For McDonald spectra, the mean rotational velocity and the standard deviation are given in the fourth column and the number of lines used is shown in the last column. The absence of suitable lines prevents the calculation of  $v \sin i$  for VW Ari and CY Aqr

HD	Identification		G92 (km s <sup>-1</sup> )	Line ( $\text{\AA}$ )
	HR	GCVS		
432	21	$\beta$ Cas	69.1	4957
		V377 Cas	135.6	4957
2628	114	GN And	$16.1 \pm 1.5$	(9)
4818	238	V526 Cas	$16.1 \pm 2.7$	(9)
8511	401	AV Cet	140.5	4957
9100	432	VX Psc	135.6	4957
10845	515	VY Psc	100.9	4957
11285		VV Ari	51.8	4957
15165		VW Ari		
15550	729	UU Ari	173.9	4957
17093	812	UV Ari	68.3	4957
23156		V624 Tau	41.6	4957
23567		V534 Tau	98.6	4957
23728	1170	V376 Per	102.1	4957
24550		V479 Tau	132.4	4957
24809	1223	V386 Per	129.4	4957
24832	1225	DI Eri	126.4	4957
26322	1287	IM Tau	$6.8 \pm 1.6$	(9)
26574	1298	<i>o</i> Eri	99.7	4957
27397	1351	V483 Tau	102.1	4957
27459	1356	V696 Tau	81.6	4957
27628	1368	V775 Tau	$32.0 \pm 4.0$	(7)
28024	1392	<i>v</i> Tau	205.1	4957
28052	1394	V777 Tau	195.7	4957
28319	1412	TH2 Tau	66.7	4957
28910	1444	$\rho$ Tau	126.4	4957
30780	1547	V480 Tau	98.6	4957
33959	1706	KW Aur	$28.1 \pm 1.5$	(9)
37819		V356 Aur	$22.5 \pm 2.2$	(9)
40372	2100	V1004 Ori	70.8	4957
40535	2107	V474 Mon	$18.8 \pm 1.5$	(9)
		UZ Lyn	60.4	4989
50018	2539	OX Aur	134.0	4957
50420	2557	V352 Aur	$26.3 \pm 2.8$	(9)
55057	2707	V571 Mon	135.6	4957
64191		AD Cmi	$12.0 \pm 2.4$	(9)
73857		VZ Cnc	$13.3 \pm 2.8$	(8)
110377	4824	GG Vir	180.0	4957
152830	6290	V644 Her	$15.6 \pm 1.8$	(6)
		V645 Her	50.2	4989
155514	6391	V620 Her	191.1	4957
156697	6434	V2112 Oph	188.9	4957
159223		V648 Her	130.9	4957
172748	7020	$\delta$ Scu	30.1	4989
177392	7222	LT Vul	135.6	4957
181333	7331	V1208 Aql	50.8	4957
181577	7340	$\rho 1$ Sgr	81.6	4957
186357	7501	V1276 Cyg	103.3	4957
192518	7731	NU Vul	205.1	4957
197461	7928	$\delta$ Del	29.4	4989
199124	8006	EM Aqr	132.4	4957
199908		DQ Cep	57.9	4957
200356		FN Aqr	41.9	4989
200925		V1719 Cyg	31.19	4989
201707	8102	EW Aqr	134.0	4957
204188	8210	IK Peg	36.9	4989
211336	8494	$\epsilon$ Cep	97.4	4957
213534	8584	GX Peg	46.2	4989
215874	8676	FM Aqr	99.7	4957

**Table 3.** continued

HD	Identification		G92 (km s <sup>-1</sup> )	Line (Å)
	HR	GCVS		
218549		DY Peg	23.6 ± 8.3	(2)
		CC And	14.5 ± 1.3	(7)
		GP And	11.5 ± 2.8	(9)
		AI Hya	132.5	4957
		CY Aqr		
		DE Lac	31.5	4989
		V1162 Ori	46.4 ± 4.0	(4)
		EH Lib	13.3 ± 1.9	(9)
		YZ Boo	18.8 ± 4.1	(5)

greatest difference in the McDonald spectra. The results are given in Table 5. We can see how the influence of the limb-darkening coefficient in the calculated value of  $v \sin i$  increases when the rotational velocity increases. For McDonald spectra, where  $v \sin i$  is always  $\leq 40$  km s<sup>-1</sup>, this effect is negligible. On the other hand, for La Palma spectra, where the difference ( $\epsilon_{\text{Wade}} - 0.6$ ) is, at worst, 0.07 this effect can also be neglected.

**Fig. 1.** Relation between the ratio of the variations in intensity of H $\alpha$  at two wavelengths ( $\lambda 6567.19$  Å and  $\lambda 6578.46$  Å) and the effective temperature

The determination of the local continuum is another unavoidable source of error: a displacement in the continuum level can change the line profile, especially the wings, and thus distort the shape of the Fourier transform and modifying the position of its zeroes. Despite of the excellent signal-to-noise ratio of the La Palma spectra, their moderate resolution and the high number of lines present in the spectral region considered make most of the lines appear blended which makes difficult the continuum placement. The error in the continuum determination for these spectra has been estimated by comparing equivalent widths of different lines in the observed spectrum of

Procyon with those from the Atlas of Procyon (Griffin & Griffin 1979). An error in the continuum positioning of 1 – 2% was adopted which correspond to an error of 8 – 10 km s<sup>-1</sup> in  $v \sin i$  for those stars with the highest rotational velocities, the error being lower when  $v \sin i$  is lower. For McDonald spectra, where the continuum is much better defined, the error associated with the continuum level indetermination is negligible.

The equivalent width of the line also plays an important role in the accuracy of the  $v \sin i$  value. This can be easily understood by considering that the peak of the main lobe in the transform corresponds to the equivalent width of the spectral line and the sidelobes are proportional to the main lobe. A large equivalent width will thus mean large amplitudes in the data transform and large relative height of the main lobe and sidelobes to the noise level.

The sampling frequency is another limiting factor in the calculation of  $v \sin i$ . Defining this frequency as  $\sigma_N = 0.5/\Delta\lambda$  and considering La Palma and McDonald spectral resolution we can get a lowest  $v \sin i$  value of  $\approx 29.5$  km s<sup>-1</sup> and  $\approx 3.1$  km s<sup>-1</sup> for La Palma and McDonald spectra respectively. Hence, for stars with  $v \sin i$  lower than these values it is not possible to calculate their rotational velocities but only an upper limit.

The intrinsic nature of  $\delta$  Sct stars is another source of error: a pulsating star generates a velocity field in the line-forming region which manifests itself as a distortion in the profiles of spectral lines. Whereas radial pulsation will only produce a shift in the central wavelength of the spectral lines, velocity perturbations whose phase is a function of longitude (non-radial) will displace the contributions of the various longitudinal strips causing bumps and dips in the line profile (Walker et al. 1987). However and due to the small amplitudes of the  $\delta$  Sct stars, the influence of the line distortions on  $v \sin i$  is negligible compared to other sources of error: Kennelly et al. (1992) measured the rotational velocities of a series of spectra of  $\gamma$  Boo obtaining an standard deviation of only  $\pm 5$  km s<sup>-1</sup>.

#### 4. Determination of effective temperatures

It is firmly established that the Balmer lines are optimum indicators for  $T_{\text{eff}} \leq 8500$  K because of their virtually null gravity dependence (Smalley & Dworetzky 1993; Furhmann et al. 1994). In this work, effective temperatures for La Palma observations have been obtained from the comparisons, using a least-squares fitting technique, between the observed H $\beta$  profile and a grid of synthetic profiles generated using ATLAS8 (Kurucz 1979a). The gravity and metallicity were fixed to  $\log g = 4.0$  and  $[M/H] = 0.0$  respectively. Previous to any comparison it was necessary to convolve the synthetic spectra with the instrumental and rotational profiles. The instrumental profile was calculated from the Thorium-Argon calibration spectra taken every night whereas the rotational profile was derived for each spectra by using Eq. (1), where

**Table 4.** Rotational velocities for the sample of non-variable stars. The value of  $v \sin i$  and the selected line(s) used for its determination are given as in Table 3

Identification	G92	Line	Identification	G92	Line		
HD	HR	(km s <sup>-1</sup> )	HD	HR	(km s <sup>-1</sup> )		
		(Å)			(Å)		
905	41	102.1	4957	203803	8190	134.0	4957
1671	82	42.2±3.4	(7)	203842	8191	80.6	4957
4568	217	10.5±2.3	(9)	203925	8198	67.5	4957
4757	230	82.5	4957	204153	8208	137.2	4957
4758	231	100.9	4957	205852	8267	195.7	4957
6397	308	6.6±0.9	(9)	205924	8270	102.8	4957
7034	349	102.1	4957	207652	8344	69.1	4957
8723	413	66.4 ± 2.3	(4)	210459	8454	135.6	4957
11257	534	14.1 ± 3.0	(9)	210594	8460	100.9	4957
11636	553	68.3	4957	210855	8472	24.6	4957
11973	569	103.3	4957	214454	8613	102.1	4957
13041	620	104.6	4957	216048	8681	81.6	4957
13161	622	60.4	4957	217754	8765	9.0 ± 1.5	(8)
13174	623	135.6	4957	217926	8776	70.5	4957
15385	723	22.3 ± 1.8	(8)	218396	8799	49.2 ± 5.4	(3)
16647	783	29.4 ± 1.8	(9)	218470	8805	11.3 ± 2.0	(9)
23230	1135	47.6 ± 2.7	(7)	219080	8830	57.9	4957
24357	1201	67.5	4957	219291	8838	81.6	4957
201507	8095	81.6	4957	219487	8845	28.3 ± 2.1	(9)
202240	8120	26.7	4989	220242	8888	7.6 ± 1.7	(9)
202444	8130	99.7	4957				

$v \sin i$  was calculated following the method described in the previous section. A step of 100 K was assumed between models.

Likewise, we tried to apply this method to McDonald observations. However, the spectral range covered by the order where H $\alpha$  appears was not wide enough to embrace the wings of the line. This produced a continuum indetermination giving rise large errors in  $T_{\text{eff}}$ . An alternative method based on the variations in intensity of the wings of H $\alpha$  at two wavelengths ( $\lambda 6517.19$  Å,  $\lambda 6578.46$  Å) was proposed. The selection of the wavelengths was done in such a way that they lie in the region of the H $\alpha$  profile with the greatest dependency with temperature. Using the set of non-variable stars and variable stars with  $\Delta V \leq 0^{\text{m}}06$  (which would correspond to a variation in temperature of  $\Delta T_{\text{eff}} \leq 100$  K, that is, the assumed step in  $T_{\text{eff}}$ ) observed in McDonald and whose temperatures were determined using H $\beta$  from La Palma spectra, we obtained a linear relationship between the intensity ratio and temperatures (Fig. 1). An error of  $\Delta T_{\text{eff}} = \pm 100$  K was assumed for La Palma spectra and  $\Delta T_{\text{eff}} = \pm 200$  K for McDonald observations.

Effective temperatures of the observed stars are displayed in Tables 6, 7. The effective temperature of UZ Lyn was not calculated using H $\beta$  since the photometric calibrations indicate a temperature  $> 8\,500$  K: at these temperatures, Balmer lines also depend on surface gravity and they cannot be used. Moreover, the effective temperature of CY Aqr has not been calculated using H $\beta$  due to the low signal-to-noise ratio which prevented us from deriving its projected rotation velocity. Also, some

**Table 5.** Influence of the limb-darkening coefficient for different rotation velocities

$v \sin i$ (km s <sup>-1</sup> )	$\Delta v \sin i$ ( $\epsilon_{0.6} - \epsilon_{0.3}$ )(km s <sup>-1</sup> )
30	0.3
60	0.8
90	0.9
120	2.2
150	4.8
180	10.1

McDonald spectra have no  $T_{\text{eff}}$  using H $\alpha$  due to problems in the flatfields of one of the nights.

#### 4.1. Comparison with integrated flux methods

The most natural way of checking the method of calculating  $T_{\text{eff}}$  based on Balmer lines would be to use it for standard stars with accurate values of  $T_{\text{eff}}$ . Code et al. (1976) and Hayes (1978) gave a list of stars with fundamentally determined values of  $T_{\text{eff}}$ . Three stars from Code et al. (1976) were also observed by us (Table 8): no systematic differences were found between the  $T_{\text{eff}}$  derived from H $\beta$  and those given in Code et al. (1976).

**Table 8.** Comparison between the effective temperatures given in Code et al. (1976) and those derived using  $H\beta$ . An error of  $\pm 100$  K was assumed for the  $H\beta$  measurements

Identification		$H\beta$	C76
HD	HR	(K)	Error
61421	2943	6600	6510 $\pm 130$ K
159651	6556	7900	8020 $\pm 330$ K
187642	7557	7800	8010 $\pm 210$ K

#### 4.2. Comparison with $T_{\text{eff}}$ derived via photometric calibrations

The temperatures obtained using  $H\beta$  have been compared with those obtained from the following *uvby* $\beta$  photometric calibrations: Petersen & Jørgensen (1972) (PJ72), Philip & Relyea (1979) (PR79), Moon & Dworetzky (1985) (MD85), Lester et al. (1986) (LGK86a,b) and Balona (1994) (B94). Except for PJ72 which relies on the scale of temperatures  $T_{\text{eff}} - (B - V)$  (Popper et al. 1970) together with the relation  $(B - V) - \beta$  (Crawford & Perry 1966), the remaining calibrations use the ATLAS8 code (Kurucz 1979a) to generate the synthetic indices and colours except for LGK86b who also used a different version of ATLAS8 (Kurucz 1979b) with a modified treatment of convection (Lester et al. 1982). Temperatures provided by the Petersen & Jørgensen (1972) and Balona (1994) calibrations have been derived using an interpolation formulae whereas temperatures calculated with the rest of photometric calibrations have been derived from grids assuming a step of 50 K. All calibrations use  $\beta$  as the temperature indicator except PR79 who use  $(b - y)$ . The  $\beta$  and  $(b - y)$  values of the  $\delta$  Sct stars have been taken from Rodríguez et al. (1994) except for UZ Lyn which does not appear in this catalogue and its values were taken from García et al. (1993). For the sample of non-variable stars the  $\beta$  and  $(b - y)$  were taken from the catalogue of Hauck & Mermilliod (1990). Both for variable and for non-variable stars, the dereddened indices were obtained using the dereddening law given by Philip & Relyea (1979). A comparison between the values of  $T_{\text{eff}}$  derived using  $H\beta$  and the photometric calibrations given above appears in Fig. 2. Those stars with variations in amplitude  $> 0^{\text{m}}06$  which would correspond to variations  $> 100$  K along the pulsation cycle were not considered.

PJ72 calculated effective temperatures which are, on average, 196 K higher than the  $H\beta$  values. These differences can be interpreted in terms of the old relationships and the few stars which this calibration is based on. In fact, these systematic differences disappear when a more modern calibration with more complete bolometric corrections and more numerous and precise

angular diameters is applied (Bohm-Vitense 1981). The effective temperatures derived from PR79 are, on average, 155 K hotter than the  $H\beta$  temperatures, this difference being larger when  $T_{\text{eff}}$  is hotter which can be attributed to the fact that only one star, Vega, with  $T_{\text{eff}}$  well outside of our range of temperatures (9 400 K), has been used in the transformation from synthetic to observed colors. MD85 provides the closest values to  $H\beta$  temperatures with a mean difference of 22 K and a standard deviation of  $\pm 116$  K, consistent with the error of  $\pm 100$  K adopted in the  $H\beta$  values whereas the mean difference between LGK86a and  $H\beta$  is  $-46$  K with a standard deviation of  $\pm 158$  K. Although this difference is not significant with respect to the assumed error in the  $H\beta$  temperatures ( $\pm 100$  K), Fig. 2 illustrates that the difference tends to be greater in the region of lower temperature. This trend can be again caused by the lack of calibration stars in our range of temperatures (only one, Procyon, and just in the edge of the interval ( $T_{\text{eff}} = 6\,500$  K)). The differences are even more relevant when the LGK86b is used (mean =  $-177$  K, std =  $\pm 157$  K). Finally, the mean difference between B94 and  $H\beta$  is 96 K with a standard deviation of 164 K. This difference shows a similar trend to LGK86a which is reasonable since B94 is based on the synthetic colours derived by Lester et al. (1986a). Moreover, the greatest differences, which appear in the interval 7 100 K – 7 800 K, can be explained in terms of how the calibration was defined: B94 used three different calibrations for three different intervals of  $T_{\text{eff}}$ :  $9\,500 \leq T_{\text{eff}} \leq 35\,000$  K;  $7\,900 \leq 9\,500$  K;  $5\,500 \leq 7\,900$  K. In this last group the calibrating stars have  $T_{\text{eff}} \leq 7\,100$  K, which means that effective temperatures in the range 7 100 K – 7 800 K were calculated by extrapolation and thus the error being greater. Moreover, we see that, for  $T_{\text{eff}} \geq 7\,900$  K, when a new calibration is used, the differences are much less significant.

## 5. Comparison with IRFM and spectrophotometric determinations

Effective temperatures derived using  $H\beta$  can be also compared with those obtained using the Infrared Flux Method (IRFM hereafter) and spectrophotometric methods. Although the lack of common observations between this paper and the papers quoted in this section prevents us from repeating the same tests done with the photometric calibrations, the similarity between  $H\beta$  and MD85 found in Fig. 2 allows us to establish comparisons by using MD85 instead of  $H\beta$ .

### 5.1. IRFM

Blackwell & Lynas-Gray (1994) (B194, hereafter) constitutes one of the most recent works on the determination of effective temperatures using IRFM. They recalculated the values given in Blackwell et al. (1990) (B190, hereafter)

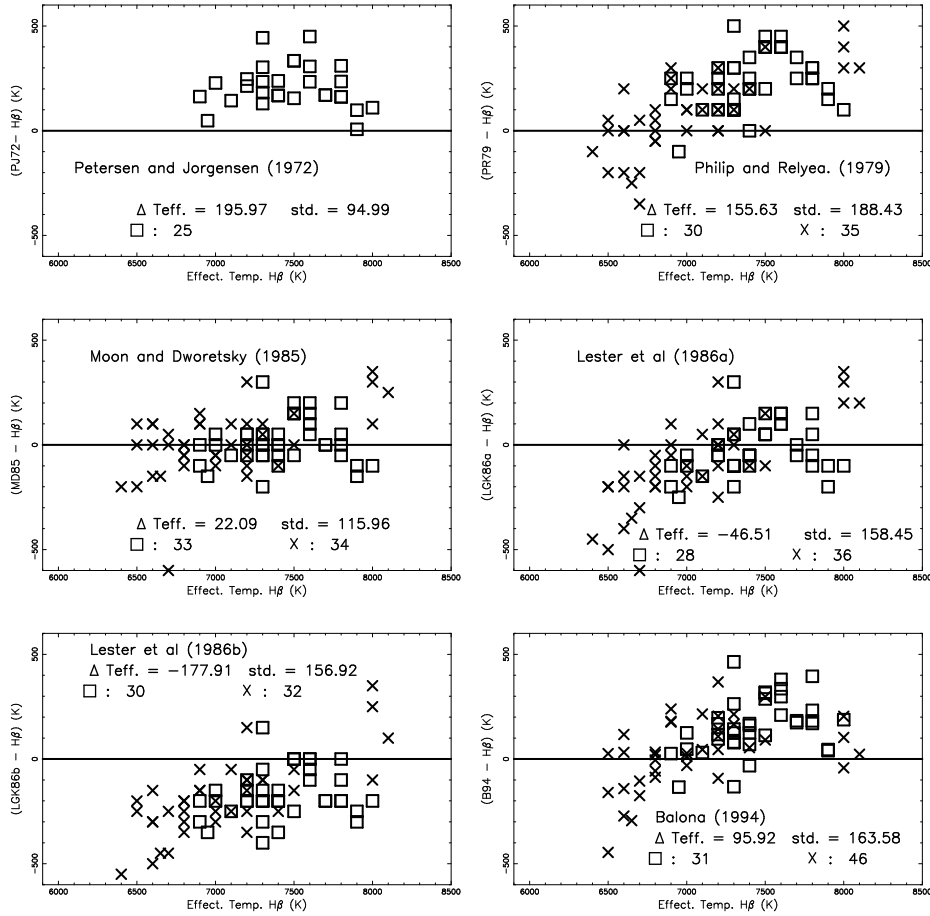


**Fig. 2.** Comparison between the values of  $T_{\text{eff}}$  calculated using  $H\beta$  and the photometric calibrations described in the text. Crosses represent non variable stars whereas squares represent  $\delta$  Sct stars. In the calibration of Petersen & Jorgensen (1972) only  $\delta$  Sct stars have been used

by using the newest version of the Kurucz models (1990, 1991, 1992) characterized by providing more accurate determinations of blanketing and ultraviolet flux than the older versions.

Figure 3 compares, for the sample of stars given in B194, the values of  $T_{\text{eff}}$  calculated with the MD85 calibration and the IRFM. As suggested by B194, an error of  $\Delta T_{\text{eff}} = \pm 150$  K has been adopted in the IRFM values, whereas an error of  $\Delta T_{\text{eff}} = \pm 100$  K has been adopted for MD85. These errors have to be understood from the point of view that the error associated to the IRFM is “absolute” in the sense that it is the result of errors in the adopted values of gravity, metallicity and interstellar extinction as well as errors in Kurucz models, especially those concerned with convection inhomogeneities and non-LTE assumptions, whereas the error of MD85 is an internal error caused by indetermination in the photometric indices which do not include errors due to the models or to the physical parameters of the stars considered as standards.

In Fig. 3 we see how the IRFM gives values which are  $\approx 100$  K systematically lower than MD85. Some authors

(Mégessier 1988; Napiwotzki et al. 1993; Smalley 1993) have found similar results suggesting two possible sources of errors: the infrared calibrations and the flux models employed. To quantify the influence of the calibration as well as the importance of the models in our range of temperatures, we have plotted in Figs. 3c and 3d the  $T_{\text{eff}}$  values of those stars in common to B194 and B190: whereas B194 used the new version of Kurucz models (1990-1992) together with Cohen et al. calibration (1992), the MARCS code of Guftasson et al. (1975) and the Dreiling & Bell (1980) calibration were employed in B190. The difference of ( $\approx 30$  K) between B190 and B194 can be explained in terms of blanketing: if blanketing increases at short wavelengths (as it happens with the new Kurucz models) the total flux conservation will make the infrared flux to be higher and, following the IRFM, the temperature lower.

## 5.2. Spectrophotometric methods

The series of papers by Malagnini et al. (1982, 1985, 1986) and Morossi & Malagnini (1985) constitute one of the most extensive works in the calculation of  $T_{\text{eff}}$  using

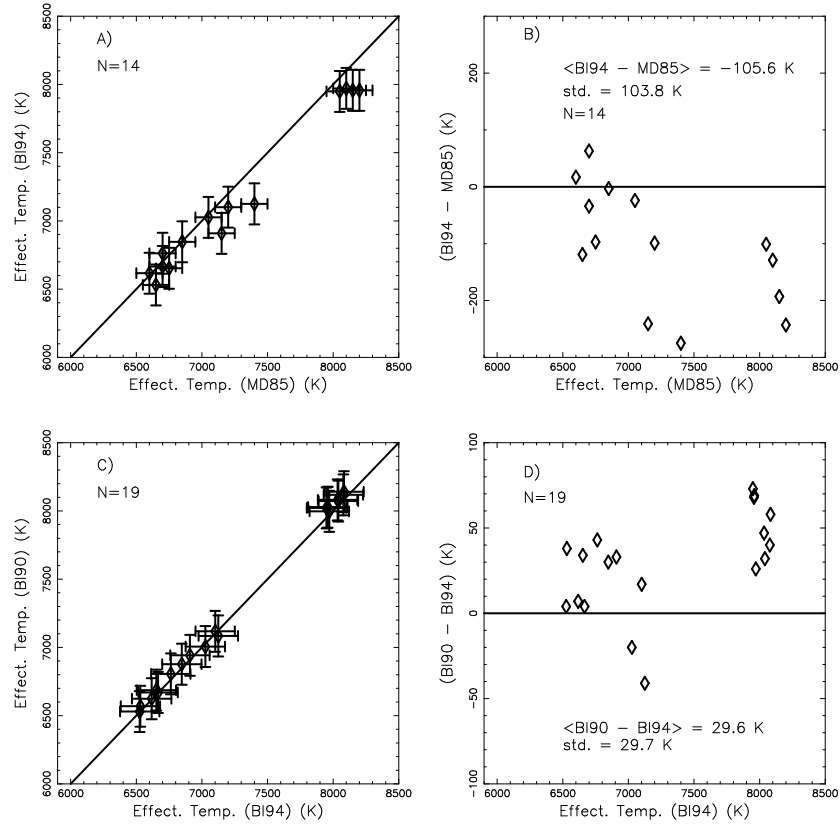


**Fig. 3.** a) Comparison between the effective temperatures calculated with MD85 and BI94. The line at 45 degrees is shown. b) Mean value and standard deviation of the difference (BI94-MD85). c) Comparison between the effective temperatures given in BI94 and BI90. The line at 45 degrees is also shown. d) Mean value and standard deviation of the difference (BI90-BI94)

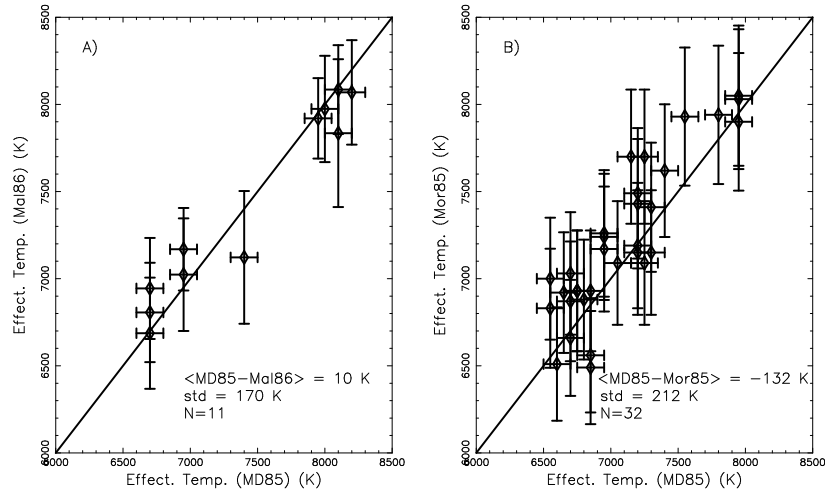


**Fig. 4.** a) Comparison between the effective temperatures calculated using MD85 and Mal 86. b) Comparison between MD85 and Mor85

spectrophotometric methods. In Fig. 4 we have compared the values of  $T_{\text{eff}}$  given in Malagnini et al. (1986) (Mal86, hereafter) and Morossi & Malagnini (1985) (Mor85, hereafter) with those values obtained from the MD85 calibration. The average difference between MD85 and Mal86 is  $10 \text{ K} \pm 170 \text{ K}$  and between MD85 and Mor85 it is  $132 \text{ K} \pm 212 \text{ K}$ . A possible explanation of the differences between the two samples found in Fig. 4b could be the adopted color excess: in the Mor85 sample, the reported values of  $T_{\text{eff}}$  depend on  $E(B - V)$  since the reddening modifies both the shape and the absolute level of the flux distribution. The color excess was measured according to the values of  $(B - V)_0$  adopted by Fitzgerald (1970). These have an associated error of 0.02 mag. which corresponds to an error in  $T_{\text{eff}}$  of  $\pm 5\%$ . To produce the systematic difference of 132 K found in Fig. 4b a deviation of  $\pm 2\%$  would be enough. Hence, we see how a slight difference in the definition of the intrinsic colors could explain the trend found in Fig. 4b. This problem is not present in Mal86 since in this case the sample is formed of bright stars with  $E(B - V) \approx 0.0$ .

## 6. Relationship between physical and pulsation parameters

### 6.1. Rotational velocity and amplitude

In Fig. 5 we have plotted the variation in amplitude of the observed  $\delta$  Scutis against their rotational velocities. Although some authors (e.g. McNamara 1985) have suggested a value of  $\Delta V = 0^{\text{m}}3$  as criterion to distinguish between low and large amplitude  $\delta$  Sct stars, from this figure we can see how a value of  $\Delta V = 0^{\text{m}}1$  represents better the border between these two subclasses.

Although from Fig. 5 we can see that both multimode ( $N = 15$ ) and single or double mode pulsators ( $N = 10$ ) are present in the low amplitude region, the presence of low amplitude single or double mode pulsators is possibly due to an insufficient number of observations: only with internationally coordinated campaigns that allow to have continuous data of a star over several weeks it has been possible to clearly identify the modes in small amplitude  $\delta$  Sct stars (Ostermann et al. 1991; Kurtz 1994). Thanks to these campaigns, stars assumed to be single mode, radial pulsators in the past are now shown as non-radial pulsators (e.g. GX Peg, Michel et al. 1992). All the stars of Fig. 5 identified as low amplitude single or double mode pulsators were observed only from a single site and for intervals of time that range from a few hours (IK Peg, Wonnacot et al. 1994) to 10 nights (OX Aur, Gupta 1980). On the contrary, the stars identified as multimode pulsators typically correspond to continuous multi-site observations performed for longer intervals of time (e.g. GX Peg, Michel et al. 1992).

On the other hand, although it has been commonly accepted that, for large amplitude  $\delta$  Scuti stars, only one

or two frequencies appear excited and that both single and double modes reveal unequivocally radial pulsation (e.g., Rodríguez et al. 1992b; Garrido et al. 1990), some other authors have suggested the presence of non-radial modes in some large amplitude  $\delta$  Scuti stars indicating that these stars might be multiperiodic with additional modes close to the limit of photometric detectability (e.g., Fu et al. 1995; Walraven et al. 1992).

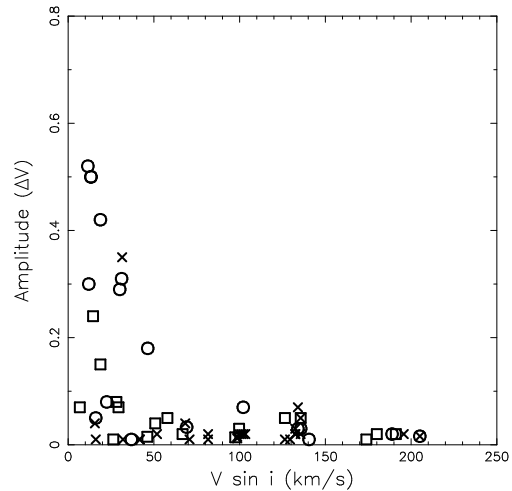


**Fig. 5.** Distribution of rotational velocities of  $\delta$  Sct stars according to their variations of amplitude. Circles represent single or double-mode pulsators (18 stars), squares multi-mode pulsators (17 stars) and crosses those stars for which no mode analysis is available (27 stars)

The idea that  $\delta$  Sct with large variations in amplitude show low rotational velocities, as it is shown in Fig. 5, was already pointed out by Danziger & Faber (1972) although their small sample did not let them draw any strong conclusion. Dziembowski (1980) suggested that, among low amplitude  $\delta$  Scuti stars, the pulsational energy is shared among the different modes by the so-called *non-linear mode coupling*: the presence of radial and non-radial modes permits the effective sharing of energy through resonances which prevent a particular pulsation mode from developing a large amplitude. This author also showed theoretically that the three-mode coupling significantly reduces the amplitude for stars with rotation velocities  $\geq 20 \text{ km s}^{-1}$  (Dziembowski et al. 1988). Taking into account that the  $v \sin i$  values derived from La Palma spectra for large amplitude stars cannot be regarded as real values but only upper limits, (Sect. 3), and relying only on those  $v \sin i$  values calculated from the McDonald sample, we can see that the limit in rotation velocity predicted by Dziembowski corresponds well with the observed limit. V1162 Ori ( $v \sin i = 46 \text{ km s}^{-1}$ ,  $\Delta V = 0.18$ ) may be an exception. However, the monopercidicity of this star needs to be more firmly established. Although due to the low signal-to-noise ratio

only four lines were used to derive the rotation velocity, the value of the standard deviation in  $v \sin i$  is only of  $4 \text{ km s}^{-1}$  which indicates that there are not important differences between the values derived from each line and the calculated rotation velocity being, thus, real. Moreover, the fact that CC And, catalogued as large amplitude  $\delta$  Scuti but with a relatively small amplitude with respect to the rest of the stars within this category ( $v \sin i = 14 \text{ km s}^{-1}$ ,  $\Delta V = 0.24$ ), also exhibits radial and non-radial modes could make us consider an intermediate stage where non-radial modes and large amplitudes can coexist.

Considering the four  $\delta$  Sct stars showing low amplitudes ( $\Delta V \leq 0.1$ ) and  $v \sin i \leq 20 \text{ km s}^{-1}$  (GN And, V526 Cas, IM Tau and V644 Her) we could think that they may be large amplitude  $\delta$  Sct stars whose amplitudes have been limited by some physical mechanism. An efficient way of reducing the pulsational amplitude is to reduce the amount of helium in the helium ionization zone: according with the diffusion theory (Baglin 1972), in a stable atmosphere helium tends to sink due to gravity which is not balanced by radiation pressure. This is the commonly adopted mechanism to explain the presence of metallic  $A_m$  stars in the instability strip. However, the abundance analysis performed on this group of  $\delta$  Scuti stars (Solano & Fernley 1997) does not indicate the presence of characteristics typical of  $A_m$  stars (i.e. calcium underabundance and iron overabundance). More probably this group can be considered as normal low amplitude multimode pulsators  $\delta$  Scuti stars seen pole-on. IM Tau is, in fact, a multimode pulsator and GN And is assumed as single pulsator but probably because of an insufficient number of observations (only three nights, Rodríguez et al. 1993b). No frequency analysis is available for V526 Cas and V644 Her. This suggestion is reinforced if a theoretical  $v \sin i$  distribution assuming random orientation of the rotation axes and Maxwellian distribution is considered (Gray 1988). In our case, for a sample of  $N = 51$  low amplitude  $\delta$  Sct stars with an average value of  $\langle v \sin i \rangle = 96.68 \text{ km s}^{-1}$ , the theoretical distribution gives  $\approx 3$  stars with  $v \sin i \leq 20 \text{ km s}^{-1}$  which is quite close to the observed number.

In order to find out whether the distribution of the  $v \sin i$  values of the low amplitude  $\delta$  Sct stars resembles that of non-variable stars, we proposed to apply the Kolmogorov-Smirnov test to our samples of low amplitude  $\delta$  Scutis and non-variable stars. We decided to use this test (K-S test, hereafter) since it treats the individual observations separately, thus ensuring that no information is lost because of binning (unlike other tests like the  $\chi^2$  - test).

It is well known that the A-F spectral types constitute a transition region in the distribution of rotational velocities of dwarf stars: According to Fukuda (1982) the rotational velocity is large for hot stars, it keeps constant for normal A stars dropping rapidly through the F-star region and is small for cool stars. This will cause a bias effect if both samples of stars do not show similar dis-

tributions of spectral types. In Fig. 6 we can see how the observed non-variable stars reveal a peak around F5 spectral types whereas the low amplitude  $\delta$  Scuti stars are grouped around F0. Following Fukuda (1982) this would correspond to a difference of  $\approx 80 \text{ km s}^{-1}$  in  $v \sin i$ . The fact that the non-variable stars show significantly lower values of  $v \sin i$  than the low amplitude  $\delta$  Sct stars will affect the cumulative distributions functions making the K-S test not valid. To solve this problem, we have compared only the normal A-stars in both samples (Fig. 7). However, there are only 6 normal A-stars in the non-variable sample and for the sake of statistical significance, we would like to have data samples as large as possible. In an attempt to improve this situation, we have added those low amplitude  $\delta$  Sct stars with known  $v \sin i$  given in Rodríguez et al. (1994). At the same time, the sample of non-variable stars has been completed with stars from Hoffleit (1982) in such a way that both the low amplitude  $\delta$  Sct and the non-variable samples have the same number of stars ( $N = 105$ ) and show the same spectral type distribution. Those peculiar stars ( $A_m, A_p, \dots$ ) which could have biased the  $v \sin i$  distribution were not considered. Although two different catalogues have been used for the spectral type identification (Rodríguez et al. (1994) for the  $\delta$  Sct stars and Hoffleit (1982) for the non-variable stars) we did not find significant differences between them after comparing the spectral types of the set of stars in common with both catalogues. On the other hand, the  $v \sin i$  values of our observed stars (both  $\delta$  Sct and non-variables) were calculated following the method described in Sect. 3 whereas the values of the stars added to both samples were taken from Uesugi & Fukuda (1982). A comparison between our  $v \sin i$  values and those given in Uesugi & Fukuda (1982) does not yield systematic differences which could affect the statistical analysis. In Fig. 7 we compare the histograms of both samples as well as their correspondent cumulative distribution functions. The null hypothesis adopted in the K-S test (the two data set are drawn from the same distribution function) can be rejected with a 98% of confidence level. In this figure we can see that the  $\delta$  Sct stars show a broader distribution in rotation velocity than the non-variable stars. Also, the average rotation velocity is higher for  $\delta$  Sct stars than for non-variable stars which agrees with Breger (1979). Although this author suggested that the differences may be caused by the inclusion of  $A_m$  stars this is not our case since only normal A-star have been considered. Moreover, in Fig. 7 we can see that up to  $100 \text{ km s}^{-1}$  the cumulative distribution of  $\delta$  Sct and non-variable stars are quite similar, the differences being present for  $v \sin i \geq 100 \text{ km s}^{-1}$ . This lead us to think that high rotation may increase the probability of  $\delta$  Scuti pulsation.

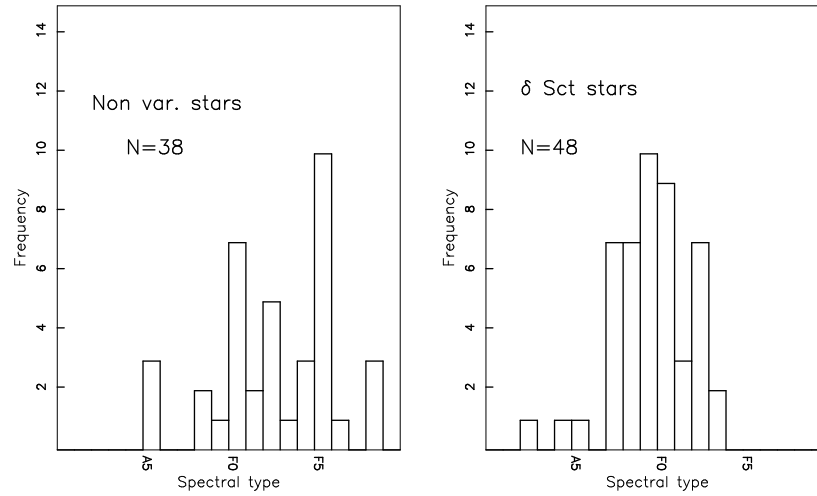


**Fig. 6.** Distribution of the sample of observed low amplitude  $\delta$  Sct and non-variable stars according to their spectral type

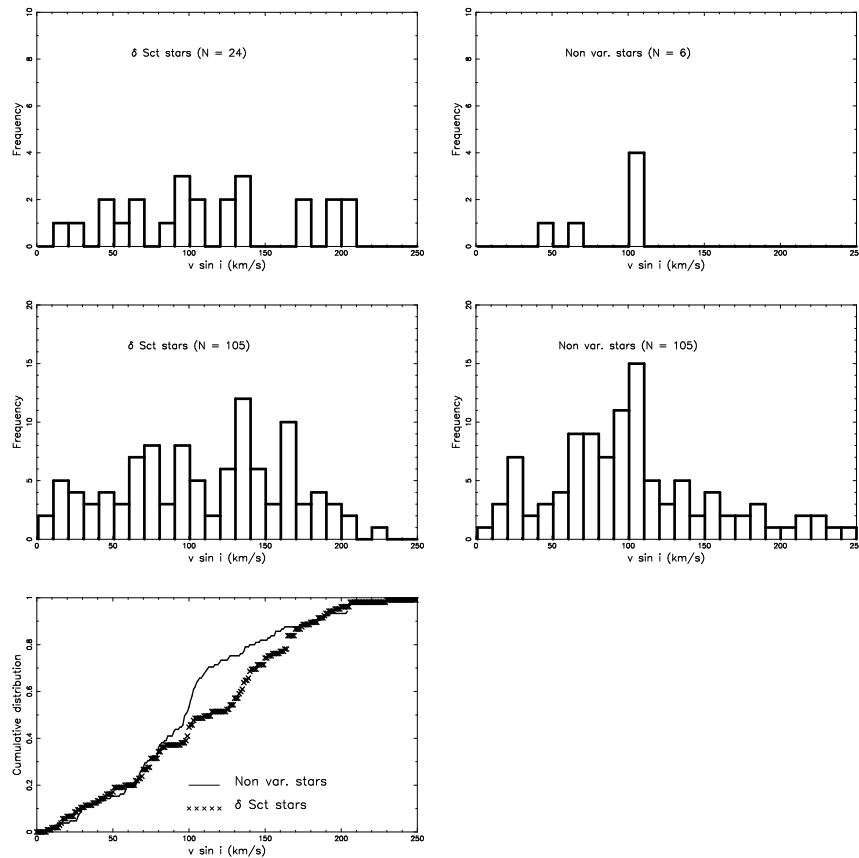


**Fig. 7.** Distribution of the observed A-spectral type  $\delta$  Scuti and non-variable stars according to their projected rotational velocity (upper panels). Distribution of the extended samples of  $\delta$  Scuti and non-variable stars (middle panels) and their cumulative distributions (lower panel)

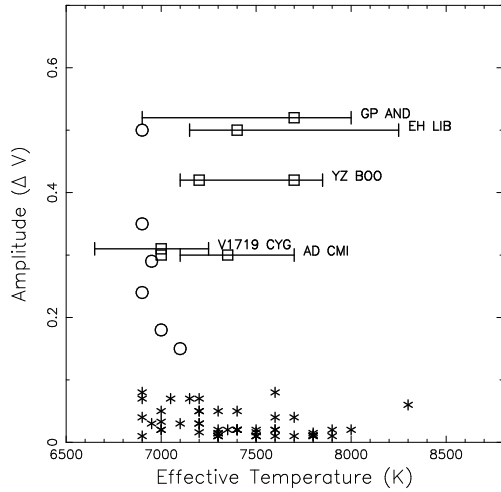


**Fig. 8.** Distribution of effective temperatures for low (asterisks, 51 stars) and large amplitude (circles, 6 stars and squares, 7 stars)  $\delta$  Sct stars derived from our  $H\beta$  measurements. The circles represent mean effective temperatures along the pulsation cycle whereas the squares are the temperatures derived from  $H\beta$  at a given phase. The horizontal bars represent the whole range of temperatures for those large amplitude  $\delta$  Scutis with  $uvby\beta$  photometry available over a pulsation cycle. The  $uvby\beta$  values are from Rodríguez et al. (1993a, GP And), Jøner (1986, EH Lib), Jøner & McNamara (1983, YZ Boo), Johnson & Jøner (1986, V1719 Cyg) and Kim & Jøner (1994, AD CMi)

### 6.2. Effective temperature and amplitude

In Fig. 8 we have plotted the effective temperature of both low and large amplitude  $\delta$  Scuti stars versus the amplitude variation. In both cases, the  $T_{\text{eff}}$  values have been derived from our  $H\beta$  measurements. Moreover, for those large amplitude stars with  $uvby\beta$  photometry available in the literature, the whole range of temperatures over a pulsation cycle has been also calculated using the MD85 calibration. We have applied the K–S test to compare the effective temperatures of the samples of low amplitude and large amplitude with  $uvby\beta$  photometry (mean  $T_{\text{eff}}$  along the cycle). Although due to the small number of large amplitude stars considered we cannot conclude from the K–S test that both samples are drawn from different distributions, Fig. 8 seems to indicate that large amplitude stars tend to have lower effective temperatures. This result is consistent with Breger (1980) who suggest that large amplitude  $\delta$  Sct stars are more evolved stars crossing the Instability Strip at higher luminosities and therefore, on average, cooler temperatures. The scarcity of the large amplitude  $\delta$  Scutis compared to the low amplitude (Rodríguez et al. 1994) also support this hypothesis.

### 6.3. Period versus $v \sin i$ and effective temperature

In Fig. 9a we show the distribution of periods for the  $\delta$  Sct stars given in Rodríguez et al. (1994). In the multiperiodic stars we have only considered the period which corresponds to the dominant radial pulsation mode in every case. In this figure we can see that large amplitude stars tend to have longer periods: the K–S test predicts that the hypothesis that both samples are drawn from the same distribution can be rejected with a 99.9% of confidence level. Although, as Rodríguez et al. (1994) pointed out, there may be in this figure selection effects since low amplitudes are difficult to detect in stars with long periods because of the photometric stability required to get precise light curves, these results agrees with the idea proposed by Breger that large amplitude  $\delta$  Sct stars are evolved stars: from the period-mean density relation we get that  $P \propto L^{3/4} / (M^{1/2} * T^3)$ , where  $P$  is the period and  $L$ ,  $M$  and  $T$  the luminosity, mass and effective temperature of the star respectively. From this relation we can see that the decrement in temperature of the post-main sequence phase of evolution would produce an increment of the period.

In Fig. 9b we also plotted the relations between the period and  $v \sin i$  and effective temperature. Whereas no correlation is found between  $v \sin i$  and period a clear relation is shown up between  $T_{\text{eff}}$  and period: the period is shorter when the temperature is higher. This relation can be easily understood in terms of the amplitude–temperature–period relation described above: low amplitude tend to have higher temperature and shorter periods than large amplitude  $\delta$  Sct stars.

## 7. Conclusions

Projected rotational velocities ( $v \sin i$ ) and effective temperatures have been derived for 68  $\delta$  Sct stars as well as for 41 non-variable stars in order to relate the physical parameters of a star with its pulsation parameters. Rotational velocities were calculated using the method developed in Gray (1992) which works well for spectra with moderate resolution and good signal-to-noise.

Effective temperatures were determined by comparing observed  $H\beta$  profiles with the theoretical profiles of Kurucz (1979a). Extensive comparison was then made between these temperatures and those derived using other methods (Infrared Flux Method, spectrophotometric methods and  $uvby\beta$  photometric calibrations). A systematic difference of 100 K between the effective temperatures obtained using the  $H\beta$  line and the IRFM (Blackwell & Lynas-Gray 1994) was found. No significant differences were found between the effective temperatures derived from  $H\beta$  and from spectrophotometric methods (Malagnini et al. 1986). The level of agreement with temperatures from  $uvby\beta$  photometry depend on the

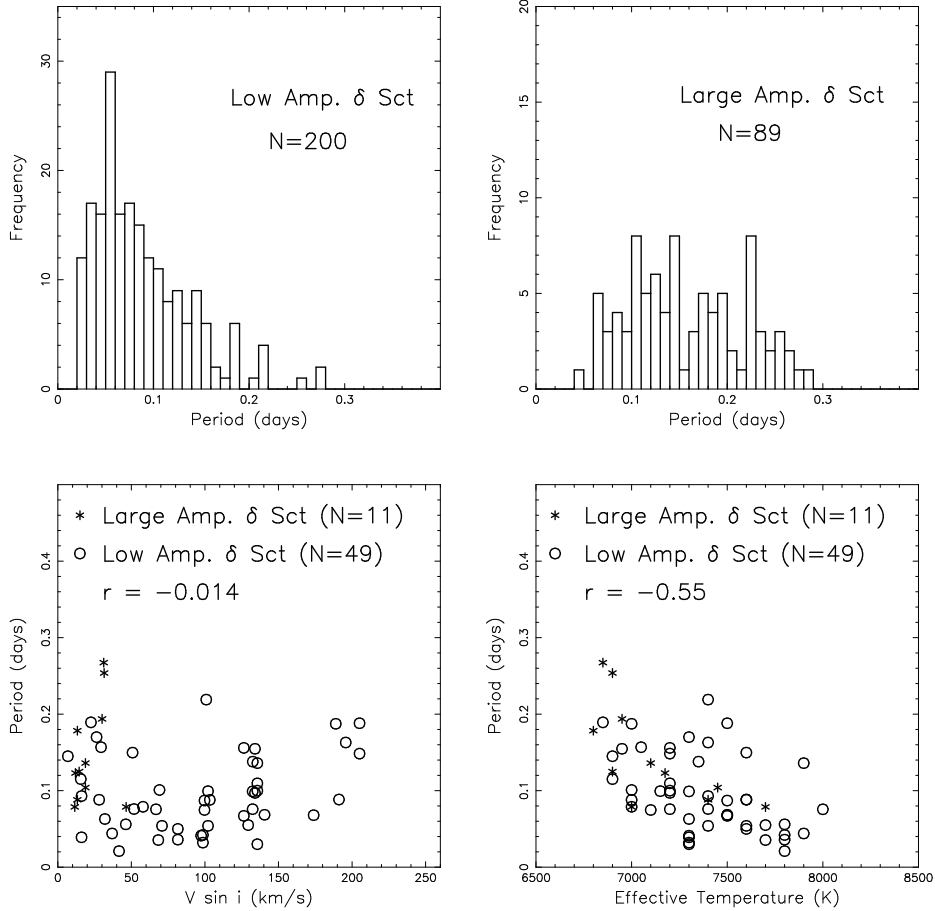


**Fig. 9. a)** Histograms of the periods of low and large amplitude  $\delta$  Sct stars (upper panels). **b)** Distribution of projected rotational velocities and effective temperatures of low and large amplitude  $\delta$  Sct stars according the period (lower panels). The correlation coefficient,  $r$ , is shown for both samples

calibration used, the best agreement being with the Moon & Dworetzky calibration (1985).

In the second part of this paper we relate  $v \sin i$  and  $T_{\text{eff}}$  with the amplitude and period of the stars. There is a clear relation between amplitude and  $v \sin i$  with all the large amplitude pulsators having low rotation velocities. Where modes are known, the large amplitude stars are single or double-mode radial pulsators whereas the low amplitude stars are multimode pulsators with both radial and non-radial modes excited. The multimode behaviour among low amplitude stars is consistent with the suggestion by Dziembowski (1980) that non-linear coupling between radial and non-radial modes limits the amplitudes. Several stars seem to be anomalous: V1162 Ori is a radial large amplitude pulsator with  $v \sin i = 46 \text{ km s}^{-1}$  whereas GN And is a single-mode low amplitude pulsator. In both cases, more extensive observing runs could indicate the presence of new frequencies. Moreover CC And, a multimode large amplitude star ( $\Delta V = 0.24$ ), may indicate an intermediate stage where multimode pulsation and relatively large amplitude can coexist.

Comparing the distribution in  $v \sin i$  of low amplitude  $\delta$  Scutis and non-variable stars of the same spectral type, this shows a broader distribution for the  $\delta$  Scutis, suggesting that high rotation may excite pulsation.

Comparing the period-temperature relations for the large and low amplitude stars suggests that the large amplitude stars are preferentially cooler and have longer periods. From their values of  $v \sin i$ ,  $T_{\text{eff}}$ , period and their relative scarcity, the explanation proposed by Breger (1980) that the large amplitude  $\delta$  Sct stars are more evolved (sub-giants) than the low amplitude  $\delta$  Scutis (main sequence or early post-main sequence) is consistent with observation.

*Acknowledgements.* We would like to thank Rafael Garrido for helpful comments. The authors would also like to acknowledge the constructive comments of an anonymous referee. This work has made use of the Simbad database, operated at CDS, Strasbourg, France.

## References

- Baade D., Bardelli S., Beaulieu J.Ph., Vogel S., 1992,  $\delta$  Scuti Newslett. 5, 3
- Baglin A., 1972, A&A 19, 45
- Balona L.A., 1994, MNRAS 268, 119
- Balona L.A., Stobie R.S., 1980, MNRAS 190, 931
- Bartolini C., Dapergolas A., Piccioni A., Voli M., 1980, IAU Inform. Bull. Var. Stars 1757, 1
- Bessell M.S., 1969, ApJS 18, 195
- Blackwell D.E., Lynas-Gray A.E., 1994, A&A 282, 899
- Blackwell D.E., Petford A.D., Arribas S., Haddock D.J., Selby M.J., 1990, A&A 232, 396
- Böhm-Vitense E., 1981, ARA&A 19, 295
- Bossi M., Guerrero G., Mantegazza L., Scardia M., 1983, A&ASS 53, 395
- Bossi M., Guerrero G., Mantegazza L., Scardia M., 1983, Ap&SS 89, 429
- Breger M., 1979, PASP 91, 5
- Breger M., 1980, ApJ 235, 153
- Breger M., 1982, PASP 94, 845
- Breger M., Garrido R., Huang L., Jiang S.-Y., Guo Z.-H., Frueh M., Paparo M., 1989, A&A 214, 209
- Breger M., Ostermann W.M., Shi-Yang J., Zhi-Ping L., Akan M.C., Evrens S., Ibanoglu C., Keokin V., Tunca Z., 1994, A&A 289, 162
- Coates D.W., Moon T.T., Thompson K., Winsall M.L., 1982, IAU Inform. Bull. Var. Stars 2238, 1
- Code A.D., Davis J., Bless R.C., Hanbury-Brown R., 1976, ApJ 203, 417
- Cohen M., Walker R.G., Barlow M.J., Deacon J.R., 1992, AJ 104, 1650
- Collins G.W., Truax R.J., 1995, ApJ 439, 860
- Crawford D.L., Perry C.L., 1966, AJ 71, 206
- Díaz-Cordovés J., Giménez A., 1992, A&A 259, 227
- Danziger I.J., Faber S.M., 1972, A&A 18, 428
- Dreiling L.A., Bell R.A., 1980, ApJ 241, 736
- Dziembowski W., 1980, Lect. Not. Phys. 125, 22
- Dziembowski W., Królikowska M., Kosovitchev A., 1988, Acta Astron. 38, 61
- Eggen O.J., 1971, PASP 83, 251
- Eggen O.J., Iben I., 1989, AJ 97, 431
- Fernley J.A., Jameson R.F., Sherrington M.R., Skillen I., 1987, MNRAS 225, 451
- Fitch W.S., 1981, ApJ 249, 218
- Fitzgerald M.P., 1970, A&A 4, 234
- Fu J.-N., Jiang S.Y., 1995, A&AS 110, 303
- Fukuda I., 1982, PASP 94, 271
- Fuhrmann K., Axer M., Gehren T., 1994, A&A 285, 585
- García J.R., Cebal J.R., Scoccimarro E.R., et al., 1993,  $\delta$  Scuti Newslett. 6, 14
- Garrido R., García-Lobo E., Rodríguez E., 1990, A&A 234, 262
- González-Bedolla S.F., Rolland A., Rodríguez E., López de Coca P., 1990, IAU Inform. Bull. Var. Stars 3533, 1
- Gray D.F., 1992, in: The observation and analysis of stellar photospheres. Cambridge Univ. Press, p. 368
- Gray D.F., 1988, in: Lectures on Spectral-Line Analysis: F,G and K stars. Aylmer Express Ltd., chapter 5
- Griffin R., Griffin R., 1979, in: A photometric atlas of the spectrum of Procyon  $\lambda\lambda 3140 - 7470 \text{ \AA}$ . The Observatory, Cambridge
- Gupta S.K., 1980, Ap&SS 68, 423
- Gustafsson B., Bell R.A., Eriksson K.E., Nordlund A., 1975, A&A 42, 407
- Hauck B., Mermilliod M., 1990, A&AS 86, 107
- Hayes D.S., 1978, in: Philip A.G., Davis & Hayes, Reidel D.S. (eds.) Proc. IAU Symp. 80, The HR diagram. Dordrecht, Holland
- Hobart M.A., Pena J.H., Peniche R., 1989, Rev. Mex. Astron. Astrofis. 17, 103
- Hoffleit D., Jaschek C., 1982, in: The Bright Star Catalogue, Yale University Observatory
- Horne K., 1986, PASP 98, 609
- Johnson S.B., Joner M.D., 1986, PASP 98, 581
- Joner M.D., 1986, PASP 98, 651
- Joner M.D., McNamara D.H., 1983, PASP 95, 433
- Kenelly E.J., Yang S., Walker G.A.H., Hubeny I., 1992, PASP 104, 15
- Kim C., Joner M.D., 1994, A&ASS 218, 137
- Klinglesmith D.A., Sobieski S., 1970, AJ 75, 175
- Kukarkin B.V., Kholopov P.N., Efremov Y.N., et al., 1969, in: General Catalogue of Variable Stars, Moscow
- Kurtz D.W., 1994, Delta Scuti Star Newslett. 7, 13
- Kurucz R.L., 1979a, ApJS 40, 1
- Kurucz R.L., 1979b, in: Dudley Obs. Rept. 14, 271
- Kurucz R.L., 1990, in: Hansen J.R. (ed.) Atomic Spectra and Oscillator strengths for Astrophysics and Fusion Research. North-Holland, Amsterdam, p. 20
- Kurucz R.L., 1991, in: Crivellari L., Hubeny I., Hummer D.G. (eds.) Stellar Atmospheres: Beyond Classical Models, NATO ASI Ser. C, Vol. 341, p. 441
- Kurucz R.L., 1992, in: Barbuy B., Renzini A. (eds.) The Stellar Populations of Galaxies, IAU Symp., 149, Angra Dos Reis, Brazil, p. 225
- Lester J.B., Gray R.O., Kurucz R.L., 1986, ApJS 61, 509
- Lester J.B., Lane M.C., Kurucz R.L. 1982, ApJ 260, 272
- Malagnini M.L., Faraggiana R., Morossi C., Crivellari L., 1982, A&A 114, 170
- Malagnini M.L., Morossi C., Rossi L., Kurucz R.L., 1986, A&A 162, 140
- Malagnini M.L., Morossi C., Rossi L., Kurucz R.L., 1985, A&A 152, 117
- Manduca A., Bell R.A., Gustafsson B., 1977, A&A 61, 809
- McNamara D.H., 1985, PASP 97, 715
- McNamara D.H., Feltz K.A., 1978, PASP 90, 275
- McNamara B.J., Horan S.J., 1984, APJ 282, 741
- Megessier C., 1988, A&AS 72, 551
- Michel E., Belmonte J.A., Alvarez M., et al., 1992, A&A 255, 139
- Moon T.T., Dworetzky M.M., 1985, MNRAS 217, 305
- Moore C.E., Minnaert M.G.J., Houtgast J., 1966, in: National Bureau of Standards, The Solar Spectrum 2935 Å to 8770 Å
- Morossi C., Malagnini M.L., 1985, A&AS 60, 365
- Napiwotzki R., Schönberner D., Wenske V., 1993, A&A 268, 653
- Nemec J.M., Linnell Nemec A.F., Lutz T.E., 1994, AJ 108, 222
- Nemec J.M., Mateo M., 1990, PASPC 11, 64
- Ostermann W.M., 1990, A&SS 164, 87

- Ostermann W.M., Breger M., Garrido R., et al., 1991, A&A 245, 543
- Pena J.H., Peniche R., Margrave T.E., Hobart M.A., González S.F., 1983, A&AS 51, 71
- Petersen J.O., Jørgensen H.E., 1972, A&A 17, 367
- Philip A.G.D., Relyea L.J., 1979, AJ 84, 1743
- Popper D.M., Jørgensen H.E., Morton D.C., Leckrone D.S., 1970, ApJ 161, L57
- Poretti E., 1989, A&A 220, 144
- Poretti E., Antonello E., 1988, A&A 199, 191
- Poretti E., Antonello E., Le Borgne J.F., 1990, A&A 228, 350
- Poretti E., Mantegazza L., Antonello E., 1987, A&A 181, 273
- Poretti E., Mantegazza L., Riboni E., 1992, A&A 256, 113
- Powell J.P., Joner M.D., McNamara D.H., 1995, PASP 107, 225
- Reed L.G., Welch G.A., 1988, AJ 95, 1510
- Relyea L.J., Kurucz, R.L., 1978, ApJS 37, 45
- Rodríguez E., López de Coca P., Rolland A., Garrido R., Costa V., 1994, A&AS 106, 21
- Rodríguez E., Rolland A., López de Coca P., Garrido R., González-Bedolla S.F., 1992a, A&AS 96, 429
- Rodríguez E., Rolland A., López de Coca P., 1993a, A&AS 101, 421
- Rodríguez E., Rolland A., López de Coca P., García-Lobo E., Sedano J.L., 1992b, A&AS 93, 189
- Rodríguez E., Rolland A., López de Coca P., Garrido R., Mendoza E.E., 1993b, A&A 273, 473
- Shajn G., Struve O., 1929, MNRAS 89, 222
- Slettebak A., Collins G.W., Boyce P.B., White N.M., Parkinson T.D., 1975, ApJS 29, 137
- Smalley B., 1993, MNRAS 265, 1035
- Smalley B., Dworetzky M.M., 1993, A&A 271, 515
- Smith H.J., 1955, AJ 60, 179
- Smith M.A., 1992, ApJ 254, 242
- Solano E., Fernley J., 1995 (in preparation)
- Tonry J., Davis M., 1979, AJ 84, 1511
- Uesugi A., Fukuda I., 1982, in: Revised Catalogue of Stellar Rotational Velocities, Depart. of Astronomy, Kyoto Univ., Japan
- Uyaniker B., Haykal A., 1991, IAU Inform. Bull. Var. Stars 3676, 1
- Wade R.A., Rucinski M., 1985, A&AS 60, 471
- Walker G.A.H., Yang S., Fahlman G.G., 1987, APJ 320, L139
- Walraven Th., Walraven J., Balona L.A., 1992, MNRAS 254, 59
- Wonnacott D., Kellett B.J., Smalley B., Lloyd C., 1994, MNRAS 267, 1045
- Yang D., 1992, IAU Inform. Bull. Var. Stars 3770, 1